ELSEVIER

Chemical Engineering Journal 78 (2000) 29–41

Chemical Engineering Journal

www.elsevier.com/locate/cej

Modelling pressure distribution and anode/cathode streams vapour–liquid equilibrium composition in liquid feed direct methanol fuel cells

P. Argyropoulos, K. Scott*, W.M. Taama

Chemical and Process Engineering Department, University of Newcastle upon Tyne, Merz Court, Newcastle upon Tyne NE1 7RU, UK

Received 8 May 1999; received in revised form 8 October 1999; accepted 22 October 1999

Abstract

A model is presented to predict the local pressure and chemical composition in the anode and cathode sides of a liquid feed direct methanol fuel cell. The model is based on the homogeneous two-phase flow theory and mass conservation equation, which describes the hydraulic behaviour of an experimental large cell. The model allows an assessment of the effect of the operating parameters: inlet temperature, current density, flow rates and pressure, on the pressure losses, fluid compositions and chemical equilibrium.

Keywords: Direct methanol fuel cell; Pressure distribution; Pressure drop; Modelling; Stacks

1. Introduction

Direct methanol fuel cell (DMFC) stacks are under development at a number of research group world-wide [1–7]. There are a number of scientific and technological issues yet to be solved with the DMFC before it can reach commercialisation (expected at 2008). Most of the issues concern the electrochemical problems associated with methanol oxidation, e.g. more active and cheaper electrocatalysts, membranes with reduced methanol crossover characteristics, etc., where the research effort has focused on improving the electrochemical performance of these cells [8–11]. However, there are also important engineering and design aspects that remain to be studied, which have been mainly neglected.

The design of direct methanol fuel cells and cell stacks is currently being carried out empirically or semi-empirically. There is little known about the exact nature of the phenomena that occur inside the DMFC and especially on the effect that the system design and the operating parameters have on behaviour. There is not at this time a standardised membrane electrode assembly fabrication procedure and catalyst loading, and operating conditions, vary extensively (e.g. metal loading of 2–12 mg/cm^2 has been reported and systems operating from 60–140°C, 0–5 bar pressure, 0.01–5 dm^3 min^{-1} anode side inlet flow rate, etc.) [1,3,7,9,12–17].

We have developed engineering models for DMFC stack thermal management and individual cell and overall system pressure drop [18–24]. These steady state models were based on a number of simplifying assumptions, and their main aims were to help understand the processes that occur inside a DMFC system, their interactions, and their effect on the overall system behaviour. This then enables assessment and/or improvements to be made on system design, optimal operating conditions, and to the sizing of auxiliary equipment (pumps, coolers, heaters, tanks) to operate a DMFC fuel cell stack.

Very recently several DMFC research groups presented a number of ideas:

- Very low air flow rates (close to the stoichiometric requirement) and ambient pressure operation for the cathode side with negligible power performance loss [3,7].
- Operation at 100°C with high power densities (200 mW cm^{-2} for 2.5 mg cm^{-2} metal loading) [4,5].
- A significant electrical performance improvement when operating our prototype stack system at 90°C for a specific anode side inlet flow rate range.

An effort is made to explain this kind of behaviour with the aid of the current model. The current model extends and improves our previous single cell pressure drop model which did not take into consideration the vapour–liquid equilibria in the anode flow bed, carbon dioxide solubility in the liquid

* Corresponding author. Tel.: +44-191-222-6000; fax: +44-191-222-5292.
E-mail address: k.scott@ncl.ac.uk (K. Scott)

1385-8947/00/$ – see front matter
PII: S1385-8947(99)00166-7

phase and the hydraulic resistance of the spots that comprise a significant part of the flow bed. These factors will affect significantly the pressure drop behaviour of the anode and the cathode flow beds.

The methanol water mixture has a normal boiling point (depending on the local total pressure and the mixture composition) below 100°C. Since the temperature gradient in the anode side is small for moderate inlet flow rates [21,22], the factors that control the boiling conditions are; inlet temperature, local pressure and feed composition. Hence depending on the local conditions the fuel may be boiling and the fuel cell may be operating locally as a vapour system. When this occurs, a significant improvement in the electrical performance could be expected [6]. Sundmacher et al. have presented a model of the vaporisation and phase equilibria in the anode side of the DMFC which does not include the flow bed geometry and two-phase flow behaviour and so does not provide accurate localised predictions of the composition and pressure [25,26]. When such phenomena are introduced most of the basic concepts around of which the old model was formulated are no longer valid. The current model incorporates a calculation procedure for estimating local pressures, liquid/vapour phase chemical equilibrium and local liquid/vapour fed operation.

The electrical performance of the vapour feed DMFC is still significantly higher than currently achieved for liquid fed systems. In addition, the gas diffusion electrodes currently being used for membrane electrode assembly were originally developed for gaseous systems and hence their performance is optimised for such systems. The extent of gaseous phase formation, and its exact composition, can enhance reactants penetration through these electrodes, i.e. diffusion through the gas phase in conjunction with liquid phase transport, and hence improve the overall mass transport characteristics of the cell and, thus, the overall cell performance. Furthermore, the amount of methanol vaporised is critical not only in terms of fuel utilisation but also for environmental concerns; the amount of methanol vapour that is vented to the atmosphere with the exhaust carbon dioxide should be restricted to the lowest possible level. Due to these two potential limitations of the cell it is necessary to have a model that gives information concerning the effect of the operating conditions on these two issues. Indirectly it also provides information about the effect of flow bed design on fuel utilisation and methanol recovery as it assesses the effect of local pressure variations (that can be induced from abrupt changes of the flow bed geometry) on the vapour–liquid equilibrium in the anode side two-phase flow. Finally, a prediction of the point of boiling initiation can be useful as it can be used to optimise the cell design and the operating conditions.

The ultimate goal is to merge all the four aforementioned models into a global engineering model that will be used to describe the prototype DMFC stack system under development and compare the model predictions against experimental data from our system. In the longer term such a model will be used to describe the dynamic response of such a stack.

2. Mathematical model

The present model is based on the previously published pressure drop model [18]. The flow bed geometry is directly associated with the electrochemical process occurring in the anode side electrocatalyst layer with the aid of Faraday's law. This methodology allows calculation of local mass balances and local flow composition. With the aid of these quantities and well-established chemical principles of liquid vapour equilibrium, dry gas humid volume and flash vaporisation theory, an estimation of the localised two-phase flow composition can be attempted. The incorporation of thermal and hydraulic parameters, such as local temperature, pressure and fluid friction, provides additional information concerning the effect of the overall system design and behaviour on local composition which in turn affect the cell performance. The most important theoretical aspects of the model development are briefly presented in the following paragraphs.

2.1. Methanol and water vaporisation equilibrium

It is essential to provide a calculation methodology to estimate the water and methanol vapour saturation of the anode and cathode side gas-phase at the local temperature and pressure conditions. The cell is assumed to contain liquid over its cross section, and the water vapour pressure is assumed, for simplicity, to obey Dalton's and Raoult's laws:

$$P_{H_2O} = y_{H_2O,v} P_{anode} = x_{H_2O,l}\, \gamma_{H_2O,l}\, p^{s}_{H_2O} \tag{1}$$

where $y_{H_2O,v}$ is the mole fraction of water vapour in the cathode side flow bed, $x_{H_2O,l}$ is the liquid phase mole fraction, which is a function of methanol concentration, and $p^{s}_{H_2O}$ is the vapour pressure of pure water, which is a function of temperature. The mole fraction of water is given by:

$$y_{H_2O} = \frac{p^{s}_{H_2O}(T)}{p_{anode}} \tag{2}$$

where $p^{s}_{H_2O}(T)$, in Pa, is calculated according to Wagner equation [27]:

$$\ln\left(\frac{p^{s}_{H_2O}}{P_{c,H_2O}}\right) = \left(\frac{1}{1-\chi_{H_2O}}\right)\Big(-7.76451\chi_{H_2O} + 1.45838\chi^{1.5}_{H_2O} - 2.77580\chi^{3}_{H_2O} - 1.23303\chi^{6}_{H_2O}\Big) \tag{3}$$

where

$$\chi_{H_2O} = 1 - \frac{T}{T_{c,H_2O}} \tag{4}$$

T_{c,H_2O} is water critical temperature (647.3 K) and P_{c,H_2O} water critical pressure (221.2 bar).

The air is also saturated with methanol, which again obeys Dalton's and Raoult's laws:

$$p_{\mathrm{MeOH}} = y_{\mathrm{MeOH,v}} P_{\mathrm{anode}} = x_{\mathrm{MeOH,l}}\, \gamma_{\mathrm{MeOH,l}}\, p^{\mathrm{s}}_{\mathrm{MeOH}} \quad (5)$$

where $y_{\mathrm{MeOH,v}}$ is the mole fraction of methanol vapour in the cathode side flow bed, $x_{\mathrm{MeOH,l}}$ is the liquid phase mole fraction which is only a function of the methanol concentration, and $p^{\mathrm{s}}_{\mathrm{MeOH}}$ is the vapour pressure of pure methanol which is a function of temperature.

Methanol vapour pressure can also be calculated with the aid of the Wagner equation

$$\ln\left(\frac{p^{\mathrm{s}}_{\mathrm{MeOH}}}{p_{\mathrm{c,MeOH}}}\right) = \left(\frac{1}{1-\chi_{\mathrm{MeOH}}}\right)\Big(-8.54796\chi_{\mathrm{MeOH}} + 0.76982\chi^{1.5}_{\mathrm{MeOH}} - 3.10850\chi^{3}_{\mathrm{MeOH}} - 1.54481\chi^{6}_{\mathrm{MeOH}}\Big) \quad (6)$$

where

$$\chi_{\mathrm{MeOH}} = 1 - \frac{T}{T_{\mathrm{c,MeOH}}} \quad (7)$$

$T_{\mathrm{c,MeOH}}$ is the methanol critical temperature (512.6 K) and $P_{\mathrm{c,MeOH}}$ methanol critical pressure (80.9 bar) [27].

Activity coefficients can be calculated with the aid of the Van Laar equation:

$$g^{\mathrm{E}} = A x_{\mathrm{MeOH}}\, x_{\mathrm{H_2O}} \left(x_{\mathrm{MeOH}}\frac{A}{B} + x_{\mathrm{H_2O}}\right)^{-1} \quad (8)$$

where g^{E} is the excess Gibbs energy and coefficients A and B are calculated as

$$A = RT \ln \gamma^{\infty}_{\mathrm{MeOH}} \quad (9)$$

$$B = RT \ln \gamma^{\infty}_{\mathrm{H_2O}} \quad (10)$$

and hence

$$\ln \gamma_{\mathrm{MeOH}} = \frac{A(1 + (A/B)(x_{\mathrm{MeOH}}/x_{\mathrm{H_2O}}))}{RT} \quad (11)$$

$$\ln \gamma_{\mathrm{H_2O}} = \frac{B(1 + (B/A)(x_{\mathrm{H_2O}}/x_{\mathrm{MeOH}}))^{-2}}{RT} \quad (12)$$

The only unknowns are the quantities $\gamma^{\infty}_{\mathrm{MeOH}}$ and $\gamma^{\infty}_{\mathrm{H_2O}}$ which represent activity coefficients for a binary mixture at infinite dilution. The value of activity coefficients can be calculated according to the UNIQUAC method [27]:

$$\log \gamma^{\infty}_{j} = \alpha + \varepsilon N_1 + \frac{\zeta}{N_1} + \frac{\theta}{N_2} \quad (13)$$

Values of the adjustable parameters for the binary mixture of MeOH/H_2O are presented in Table 1.

The dissolution of gases in liquid is assumed to be an equilibrium process:

$$K = \frac{p_i}{C_i} \quad (14)$$

where p is the gas partial pressure, C its molar concentration in the liquid phase and K_{c} is the Henry's law constant. Henry's law is a reasonable model of gases dissolving in liquids when concentrations and partial pressures are low. For the Henry's law constant of carbon dioxide in water a reliable average value is H=0.34 mol dm^{-3} atm^{-1} at 25°C and 1.015 bar [28]. For the case of methanol the only published information is supplied by Won, H=0.159 mol dm^3 atm^{-1} at 25°C and 1.015 bar [29].

Table 1
Correlating constants for activity coefficients at infinite dilution

Solute/solvent	T°C	α	ε	ζ	θ	N_1	N_2
MeOH→H_2O	25	−0.995	0.622	0.558	–	1	–
	60	−0.755	0.583	0.460	–	1	–
	100	−0.420	0.517	0.230	–	1	–
H_2O→MeOH	25	0.760	–	–	−0.630	–	1
	60	0.680	–	–	−0.440	–	1
	100	0.617	–	–	−0.280	–	1

The variation in the solubility of carbon dioxide in water with temperature (273–373 K) is given by Sandler [30] as

$$\ln x = -4957.824 + \frac{105288.4}{T} + 933.17 \ln T - 2.854886T + 1.480857 \times 10^{-3} T^2 \quad (15)$$

where x is the mole fraction of dissolved carbon dioxide.

Due to the lack of information on the temperature dependence of the solubility of carbon dioxide in methanol, and since at 25°C it is of the same order of magnitude as for water, the liquid mixture is considered as only water. This is considered reasonable as in practice methanol concentrations used in the DMLFC rarely exceed 2.0 mol dm^{-3}.

The model considers that the inlet feed does not contain dissolved carbon dioxide. Hence, immediately as carbon dioxide is produced from methanol oxidation it starts a process in which the gas, water and methanol, reach equilibrium. Since the mass of carbon dioxide continuously increases then at the same time the amount of water and methanol in the gas phase, which depends on the carbon dioxide mass, the local pressure, temperature and liquid phase composition, also changes. In practice methanol solution will be recycled to the cell and, therefore, the solution into the cell will potentially contain some carbon dioxide. However, since the external loop is at a different pressure and temperature than the cell itself, a separate model is required which describes the thermal management and the hydraulic behaviour of that part of the system before the inlet conditions can be precisely specified. Such a model will be incorporated in our global DMFC stack model.

The above-presented methodology is valid for liquid mixtures in equilibrium and below the liquid mixture boiling point. Closer to the boiling point of the water–methanol mixture, and especially in the case of low pressures (lower or near the atmospheric), we adopt flash vaporisation theory. A liquid mixture of known composition first boils when

$$\sum_i K_i x_i - 1 = 0 \tag{16}$$

For each component the material balance and equilibria are given by

$$Fz_i = Lx_i + Vy_i \tag{18}$$

$$y_i = K_i x_i = \begin{cases} \dfrac{\gamma_i\, p_i^{\mathrm{s}}}{P_{\mathrm{total}}} x_i & \text{for } CH_3OH \text{ and } H_2O \\ \dfrac{H_i}{P_i} x_i & \text{for } CO_2 \end{cases} \tag{19}$$

On combining these equations and introducing

$$\beta = \frac{V}{F} \tag{20}$$

which represents the fraction vaporised, the flash condition becomes

$$\sum_i x_i - 1.0 = \sum_i \frac{z_i}{1 + \beta(K_i - 1)} - 1.0 = 0 \tag{21}$$

The solution of this equation is found with the aid of a numerical scheme, e.g. the Newton–Raphson method. In that case β is found from successive approximations of the following formula:

$$\beta_j = \beta_{j-1} + \frac{\sum_i (z_i/(1 + \beta(K_i - 1)) - 1.0}{\sum_i (K_i - 1) z_i/(1.0 + \beta(K_i - 1))^2} \tag{22}$$

After β is found the phase compositions are obtained from the relationships

$$x_i = \frac{z_i}{1.0 + \beta(K_i - 1)} \tag{23}$$

$$y_i = K_i x_i \tag{24}$$

A starting value of β=1 always leads to a converged solution according to this method [31].

The aforementioned procedure is valid only when

$$\sum_1^i y_i = 1 \Leftrightarrow \sum_i K_i x_i - 1 = 0 \tag{25}$$

Successive flash vaporisations can be made on the residual liquid phase in a series of single stage operations provided that the local conditions are such that boiling takes place locally.

2.2. Pressure drop and distribution modelling

The flow bed design (Fig. 1) is based on a compact heat exchanger concept, and is divided into three sections: a triangular enlarging inlet section, 20 mm long, with a series of 2 mm^2 rectangular spots, a central region of parallel flow channels of 4 mm^2 cross section and a triangular, outlet section, of a similar design to the inlet section. Methanol solution supply to the cell is at the bottom from a 15 mm diameter inlet at one corner of the graphite plate. Methanol solution and carbon dioxide gas leave at the opposite corner at the top of the cell from a 25 mm diameter port. The cathode flow bed design for the supply of air (or oxygen) is identical to that for the anode side of the cell.

The pressure drop for the flow through that area can be calculated from

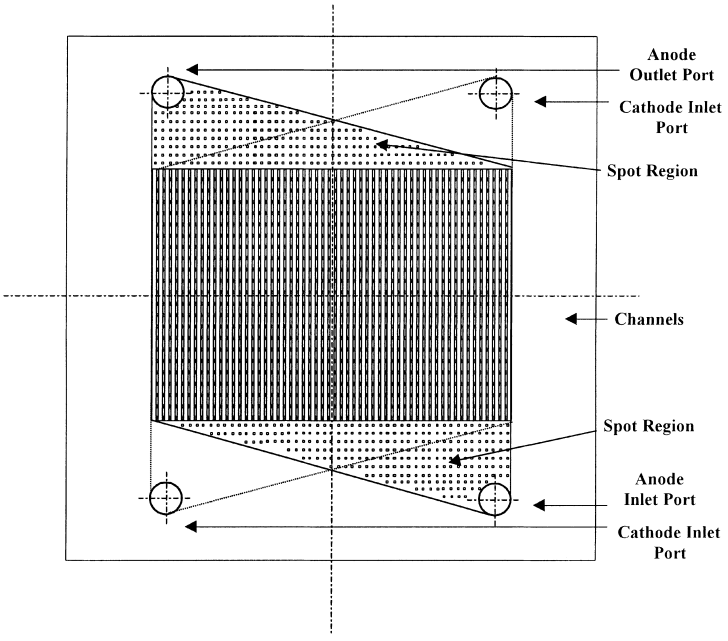

Fig. 1. Flow bed design.

$$\Delta p = \int_0^{l_1} \begin{cases} \left[G^2(y) \left[\dfrac{2(yf(y)+K_1)\upsilon_f(y)}{d_{H,ge}} + \upsilon_f(y) - \upsilon_{fi}(y) \right] + \dfrac{gy}{\upsilon_{fg}(y)} \right] dy \\ \left[G^2(y) \left[\dfrac{2(yf(y)+K_1)\upsilon_f(y)}{d_{H,ge}} \left(1 + \dfrac{x_0(y)\upsilon_{fg}(y)}{2\upsilon_f(y)} \right) + \upsilon_f(y) - \upsilon_{fi}(y) + \upsilon_{fg}(y)x_0(y) \right] + \dfrac{gy}{\upsilon_{fg}(y)x_0(y)} \right. \\ \quad \left. \times \ln\left(1 + x_0(y)\dfrac{\upsilon_{fg}(y)}{\upsilon_f(y)} \right) \right] dy \end{cases} \quad (26)$$

The first branch of this equation represents pressure drop for single-phase flow. In the second branch of Eq. (26) the first term denotes the frictional pressure drop for single phase and two-phase conditions, respectively. The second term accounts for the acceleration of the liquid due to a change in the specific volume, which produces a small pressure drop. The third term represents acceleration pressure drop for the two-phase flow. The fourth and the fifth terms of Eq. (26) denote the single phase and two-phase gravitational head, respectively. In the aforementioned formula υ_{fg} is the difference in specific volumes between the gas and the liquid phase, υ_{fi} is the liquid specific volume at the inlet temperature, υ_f is the liquid phase specific volume, and υ_g is the gas phase specific volume. All the quantities that refer to two component mixtures will be calculated as weighted averages based on the mixture mass fractions.

In the solution procedure the inlet cell pressure is initially calculated. Then the local pressure for each step is calculated with the aid of the previous step's calculated pressure drop. At the outlet of the flow bed we perform a global mass balance to calculate the liquid phase concentration and the concentration of the gaseous phase water and methanol. The first quantity is of practical importance because it can be used in a control program that will automatically replenish any methanol lost or consumed during operation. The second calculation has implications of energy efficiency and environmental protection due to the methanol vapour in the exhaust gases. It is useful in the case of adopting a strategy for methanol recovery or utilisation, e.g. electrocatalytic (or catalytic) methanol combustion, as described by Scott et al. [6]. The same procedure also applies to the cathode side where an estimation of vaporised and liquid water and methanol mass is also important for designing a water/methanol recovery and recycling system.

For the cathode side initially all the mass flows are calculated for the local temperature and pressure conditions. The methanol and water content of the air stream is calculated based on the contributions from membrane crossover and from electrochemical formation. The amount of crossover is calculated based on published values of electro-osmotic drag coefficients for water and methanol. The catalytic oxidation of methanol at the cathode side electrocatalyst is neglected as a conservative measure. This oxidation can be as high as 80% of the quantity that has passed through the membrane, although new cathode catalyst are under development which are catalytically inactive to methanol oxidation. Nevertheless, the exact amount of methanol crossover and cathode side oxidation can be calculated from specialised models, currently under evaluation [33], that are strongly dependent on the membrane electrode assembly design and the materials used. The amount of methanol crossover relative to water is small and will not significantly affect the hydraulic behaviour of the cathode. A check is performed on the mass of liquid phase water and methanol present required for the air to become fully saturated. If so, the remaining quantity of water or methanol remains in the liquid phase and a two-phase flow condition exists.

The present model attempts to quantify the relationship between the applied current density and the local two-phase flow composition along the flow channel for a wide range of potential operating conditions. Essentially, the model demonstrates the applicability of computer based modelling to the design and analysis of potential cell designs and to the estimation of the effect of operating conditions on cell performance and fuel management. Although the present results are specific to a specific stack size, the model is in all other respects generic as it provides the essential information on the interactive nature of the various electrochemical, physical, and chemical processes taking place within the cell's anode and cathode side flow beds. The model, thus, can provide feedback on specific modifications that can be made before finalising the flow bed design that would potentially improve the achieved power output.

3. Results and discussion

Initially in the anode side of the cell the liquid has to become fully saturated with carbon dioxide before formation of carbon dioxide bubbles. At a certain point in the flow bed a series of phenomena take place: a vapour–liquid equilibrium (depending on the local temperature, pressure and liquid phase composition) and hence a transition from a single-phase flow to a two-phase flow, and localised boiling of the liquid feed. It is important to know exactly at which point of the flow bed these kind of phenomena occur. Fig. 2a shows the required flow bed length for liquid phase saturation as a function of anode side inlet flow rate (0.01–1.0 $dm^3\,min^{-1}$) and of current density (50–300 $mA\,cm^{-2}$) for the following conditions; 90°C cell temperature, temperature gradient between inlet and outlet port of 0.5°C, methanol solution flow rate 0.5 $dm^3\,min^{-1}$, 100 $mA\,cm^2$, 2 $mol\,dm^{-3}$ solution, active area 270 cm^2, unless otherwise stated. Fig. 2b shows similar information for a temperature range of 85–95°C and for methanol solution concentration of 0.25–2 $mol\,dm^{-3}$. As expected the length decreases with increasing current density (i.e. more carbon

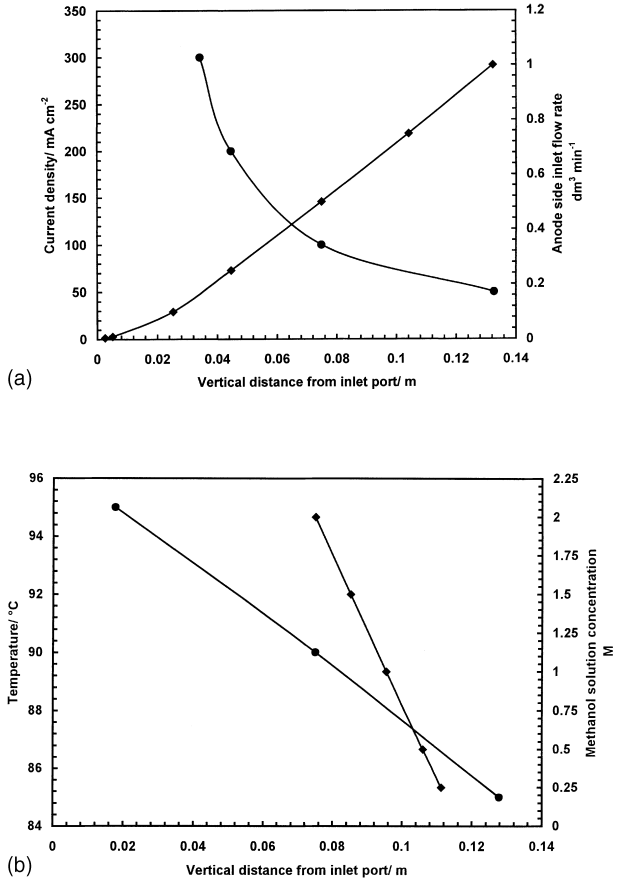

Fig. 2. Length of flow bed required to reach liquid phase saturation with carbon dioxide (90°C cell temperature, temperature gradient between inlet and outlet port of 0.5°C, 0.5 $dm^3\,min^{-1}$ 100 $mA\,cm^{-2}$, 2 M solution, active area 272 cm^2 unless otherwise stated). (a) (●) As a function of flow rates (0.01–1.25 $dm^3\,min^{-1}$): (◆) as a function of current density (50–400 $mA\,cm^{-2}$); (b) (●) As a function of temperature (80–95°C); (◆) as a function of methanol solution concentration (0.25–2 M).

dioxide is produced per unit area) and increases with increasing liquid flow rate (i.e. a larger liquid mass has to be saturated). For the aforementioned operating conditions, using a feed inlet flow rate higher than 1.0 $dm^3\,min^{-1}$ results in a single phase flow condition for the whole cell area. In practice it should be remembered that the feed solution is recycled and hence contains a certain quantity of dissolved carbon dioxide. A strong dependence of that length on the feed inlet temperature is found, as below 85°C the boiling is absent, when at 95°C the feed boils almost immediately on entry. The solution concentration, within the range considered has only a weak effect on the length before two-phase flow occurs.

We recently conducted an extensive flow visualisation study for a cell of 102 cm^2 active area [32]. This showed (Fig. 3) when operating with similar conditions a two-phase flow at the upper parts (d) for a feed flow rate above 1.0 $dm^3\,min^{-1}$. As can be seen from Fig. 3, (dark regions represent liquid flow and light regions represent gas flow) there is little visible gas formation at the lower part of the cell. The variation in length, before two-phase flow occurs, with flow rate is in reasonable agreement with the lengths that are predicted from the current model. Attention must be drawn to the fact that the cell used for modelling has an active area 2.6 times larger than the flow visualisation cell and that the feed in the flow visualisation cell was constantly recycled from a small capacity tank.

The formation of a gaseous phase results in water and methanol vaporisation. For efficient cell operation and for environmental considerations methanol must be recovered from the exhaust gas stream. Carbon dioxide release depends on the rate of the electrochemical reaction, i.e. operating current density, but the quantity of carbon dioxide in the gaseous phase strongly depends on the gas solubility in the liquid phase, which is a function of the local temperature and pressure. Since the anode side gradient is small (typically less than 1°C for high flow rates), the dominant factors are feed inlet temperature and the local system pressure. The anode side local pressure depends on the liquid phase flow rate as well as flow bed design and is practically unaffected by temperature and current density (except in the case of very low liquid phase flow rates). Fig. 4 shows the anode side pressure distribution as a function of increasing liquid phase flow rate in the case of a cell operating at 90°C, 100 $mA\,cm^{-2}$ and with a temperature gradient between inlet and outlet port of 0.5°C. The cell inlet pressure is calculated based on a reference pressure of 1.0 bar and the dynamic pressure calculated from the cell inlet flow rate and the port cross sectional area. As can be seen, pressure losses in the flow bed are not significant for the flow rates used in practice. It must be noted that the present model does not include the potentially significant pressure drops in the flow ports and that due to the presence of the spots in the triangular sections. In it's present form the model predicts that at the outlet of the cell there will be a small pressure gauge (of a few Pa). In practice although the anode side will be in a slightly elevated pressure, and also the losses will be higher, again a small gauge will be present near the cell outlet due to the presence of the sucking manifold. In general this model aims to show that the flow bed has a minimal pressure loss contribution. These small losses in the system pressure are still important in the case of multi-cell stacks. Currently our group is experimentally validating a more complicated stack model that is formulated mainly around the basic Eq. (26) but also includes the manifold losses, losses in the cell ports and also the effect of the two regions of spots.

Before proceeding to the model predictions we should stress the importance of vapour phase formation inside the anode side of a DMFC. Vapour fed DMFCs can show a superior electrical and power performance than liquid feed cells [6]. When a methanol/water vapour phase is formed it diffuses relatively easily through the carbon cloth diffusion layer (which was originally designed for vapour fed systems). The teflonised gas diffusion layer has a high degree of hydrophobicity blocking to some extent the liquid water penetration in the electrocatalytic active sites adjacent

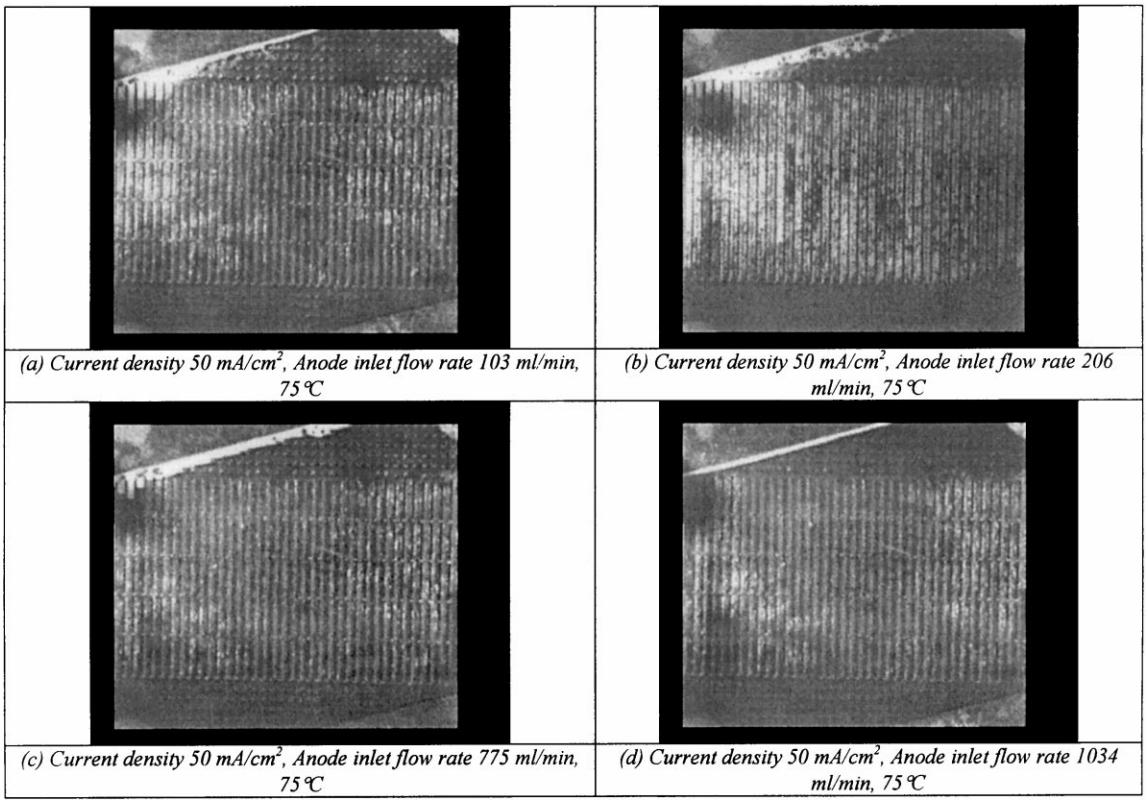

Fig. 3. Frames captured from an acrylic operating DMFC for increasing anode side liquid flow rate 0.1–1.0 $dm^3\,min^{-1}$ (75°C cell temperature, 50 mA cm^{-2}, 2 M solution, active area 102 cm^2).

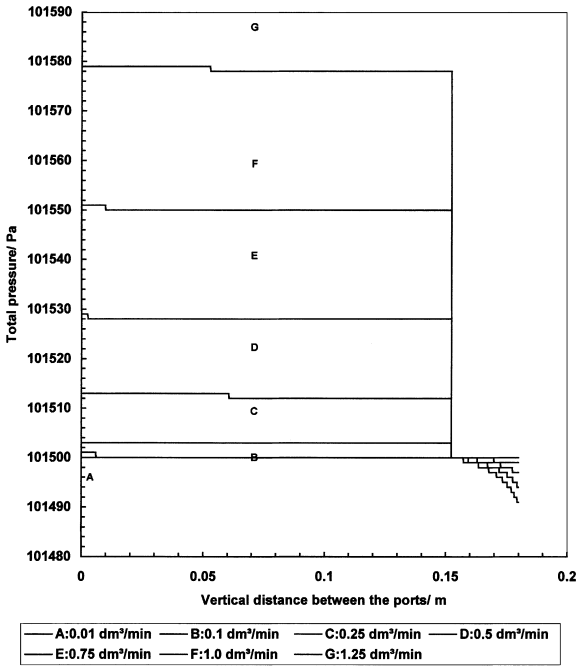

Fig. 4. Anode side pressure distribution as a function of increasing liquid phase flow rate (0.005–1.25 $dm^3\,min^{-1}$) for increasing flow bed length (90°C cell temperature, temperature gradient between inlet and outlet port of 0.5°C, 100 mA cm^{-2}, 2 M solution, active area 270 cm^2).

to the membrane. This means that the risk of flooding the active area is reduced, when at the same time reactants are supplied from the vapour phase.

3.1. Compositions of liquid and gas phases

The amounts of water and methanol vaporised depend on the amount of carbon dioxide and the local temperature, pressure, and liquid phase composition. The liquid phase composition for high flow rates, that are considered practical for the DMFC operation, vary very little due to the large feed excess. The liquid phase composition is critical for the amount of methanol present in the gaseous phase and hence affects the degree of fuel utilisation. Fig. 5a–c shows the water, methanol and carbon dioxide mole fractions in the anode side gas phase, for a range of methanol solution concentrations, as a function of increasing flow bed length (90°C cell temperature, temperature gradient between inlet and outlet port of 0.5°C, 0.5 $dm^3\,min^{-1}$ 100 mA cm^{-2}, active area 270 cm^2). Increasing the methanol solution concentration leads to a significant increase in the methanol mole fraction in the vapour phase. In addition the onset of the mixed vapour/liquid feed section is earlier in the case of the higher methanol concentrations. A penalty that would arise due to the enriched vapour phase is greater methanol crossover through the Nafion® 117 membrane, which creates a mixed potential at the cathode and lowers the electri-

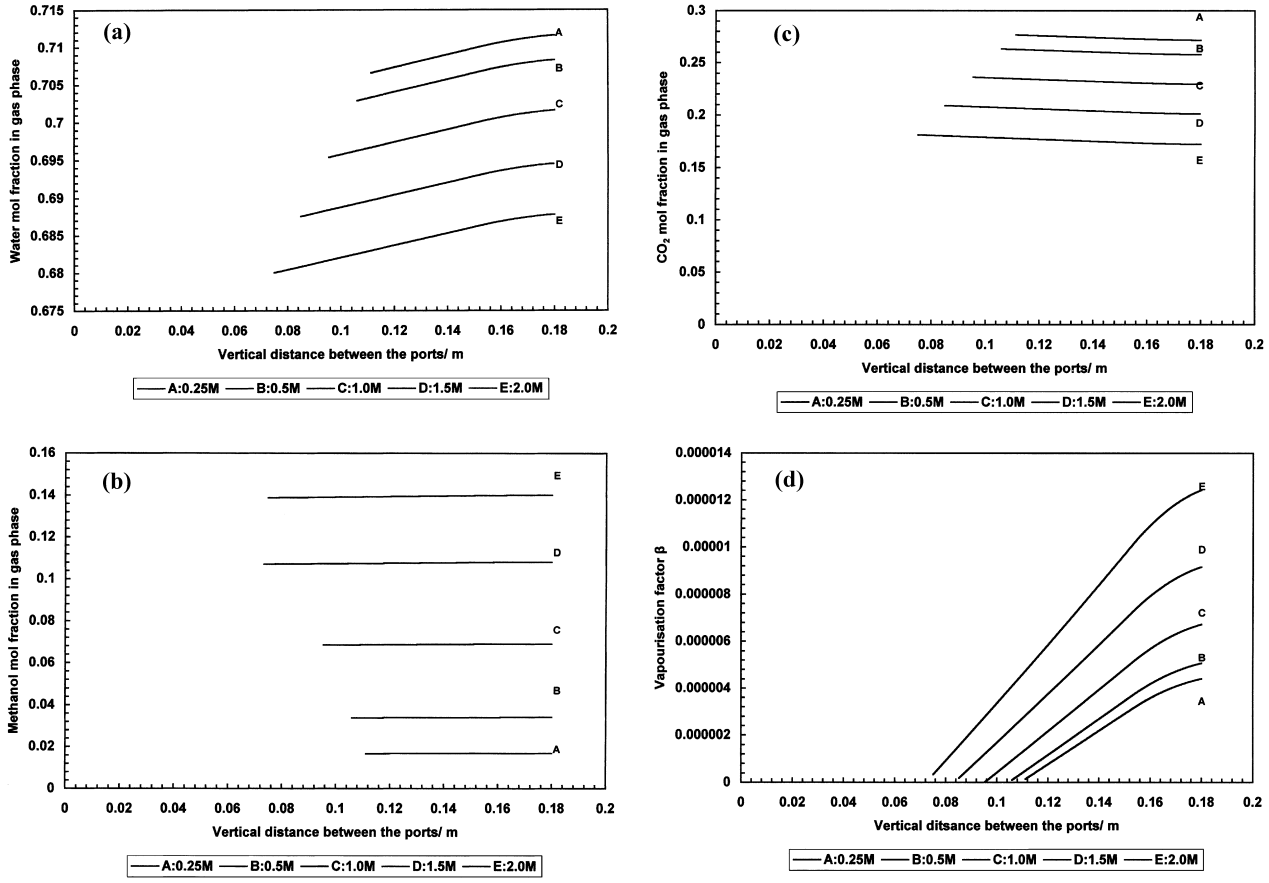

Fig. 5. (a) Water; (b): methanol; (c) carbon dioxide mole fraction β in the gaseous phase and (d) vaporisation factor for varying aqueous methanol solution concentration (0.25–2.0 M) as a function of increasing vertical distance between the ports (90°C cell temperature, temperature gradient between inlet and outlet port of 0.5°C, 0.5 $dm^3\,min^{-1}$ 100 $mA\,cm^{-2}$, active area 270 cm^2).

cal performance. Fig. 5d shows the vaporisation factor β (a measure of the ratio of the vaporised feed to the actual feed supplied in mole/mole i.e. it refers to the inlet molar flow rate of each component) for the same conditions as above. Taking under consideration the large feed excess used it can be said that the amount of feed vaporised is sufficient to maintain operation with significant current densities and power outputs. Hence, it may be that the DMFC system described by Ren [5], operated at 100°C, is internally operated as a vapour fed system, which may explain the significant power densities, reported (0.15–0.20 W/cm^2). There is experimental evidence for this in cell operation where we see that at low liquid methanol solution flow rates (1.5 $ml\,min^{-1}$ per channel) the exit fluid from the cell is predominantly a gas with some entrained liquid. The power performance at the lower flow rates is also better than that at the higher flow rates as it can be seen in Fig. 6, which shows typical variation of cell voltage and power density with flow rate.

Fig. 7a–d shows the mole fractions of water, methanol and carbon dioxide in the gas phase and the vaporisation factor β as a function of increasing vertical distance between the ports for a range of current densities 50–300 $mA\,cm^{-2}$ (A and B) and for a range of liquid phase flow rates, 0.001–1.25 $dm^3\,min^{-1}$, (C and D). In both cases increasing the current density or the liquid phase flow rate does not significantly affect the vapour phase mole fractions. On the contrary, the onset of the two-phase flow operation and the amount of the vapour phase produced is significantly affected. Overall a variety of mechanisms interact: with increased carbon dioxide production (for higher current densities) the liquid phase reaches saturation, in carbon dioxide, quite quickly and the onset of boiling starts after a few

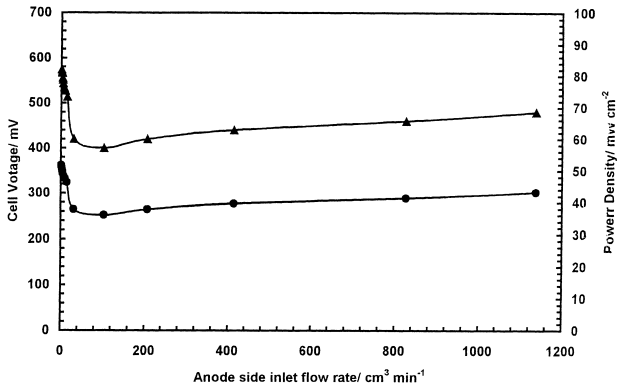

Fig. 6. The effect of methanol flow rate on the voltage, power density response of the DMFC (90°C, 2.0 mol dm^{-3} methanol, 2 bar air).

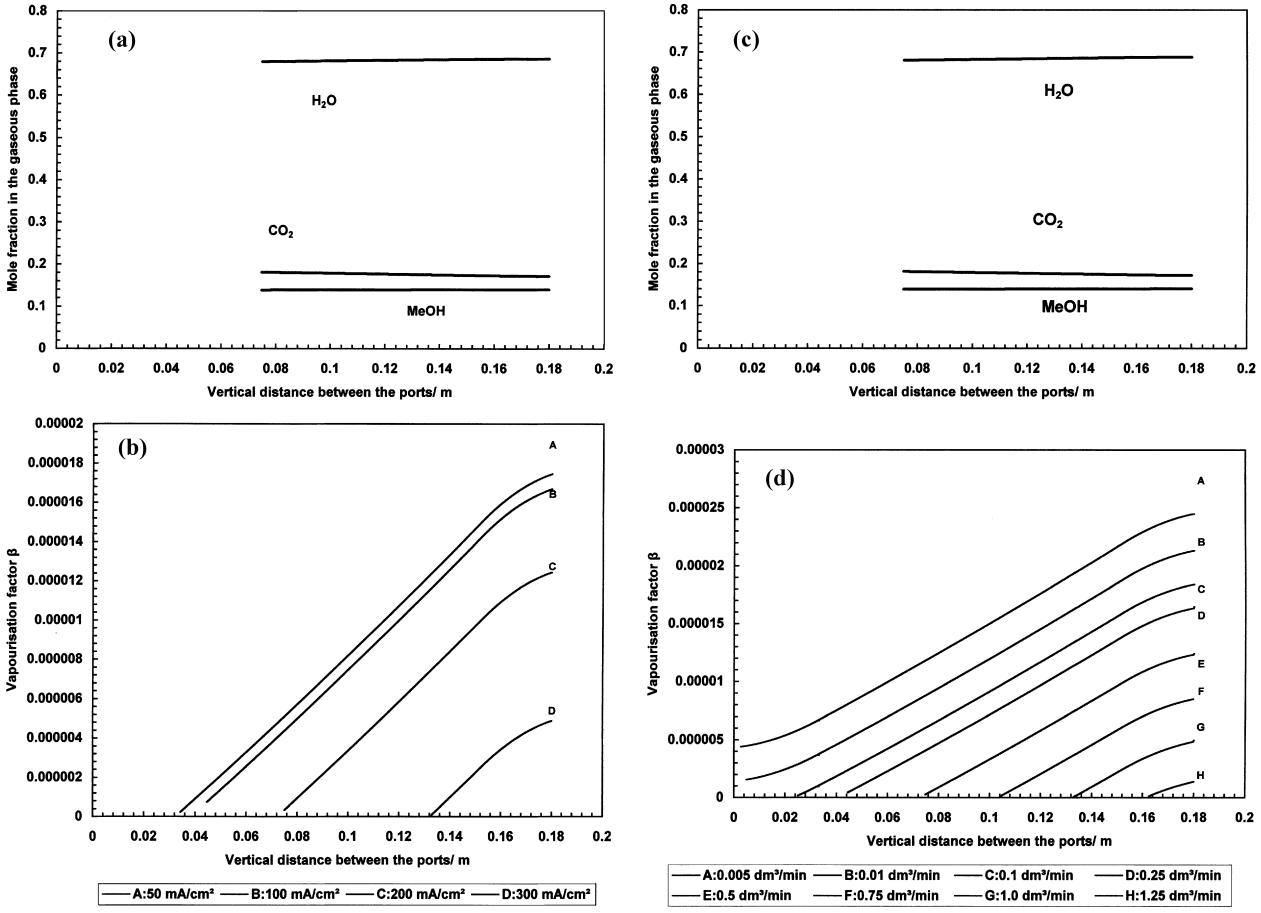

Fig. 7. Mole fractions in the gas phase and vaporisation factor β as a function of increasing vertical distance between the ports. (a) For a range of current densities (50–300 mA cm^{-2}); (b) for a range of anode side inlet flow rate of 0.005–1.25 dm^3 min^{-1} (90°C cell temperature, temperature gradient between inlet and outlet port of 0.5°C, 0.5 dm^3 min^{-1} 100 mA cm^{-2}, 2 M solution, active area 270 cm^2 unless otherwise stated).

millimetres along the flow bed. In addition a higher gas volume leads to an increase in the amount of vapour phase. In practical DMFC operation the higher current densities mean higher power densities and better power to system volume ratios but at the same time the increased vapour production results in higher methanol crossover and increased requirements for methanol recovery from the exhaust gas stream.

During laboratory studies in large DMFCs we have observed that when operating at temperatures of 90°C, or above, there was an improvement in the electrical performance for liquid phase flow rates as high as 0.25 dm^3 min^{-1}. On further increasing the liquid phase flow rate there was deterioration in performance. This latter effect was then attributed to a decrease in temperature in the anode catalyst layer, by local cooling, and also the possibility of forming a hydrodynamic layer that prohibited carbon dioxide removal from inside the catalyst layer. The present model provides an alternative explanation: at low flow rates the liquid phase carbon dioxide saturation point is reached quickly and the onset of boiling of the water methanol mixture increases the mass of vapour phase formed, with the improvement in the electrical performance that this may imply [6]. Increasing the flow rate in the intermediate region between 0.25 and 0.5 dm^3 min^{-1} decreases the boiling region in the flow bed due to the increase in the quantities of carbon dioxide required to reach the saturation point.

The authors recently reported an increase in electrical performance when operating DMFCs, operating at low temperatures (70°C) with high anode side liquid flow rates [32]. Here the high feed flow rates may serve to increase the heat transfer rate from the feed towards the catalyst layers improving the reaction kinetics. In addition the fast carbon dioxide removal from the cell at higher flow rates is another factor that potentially improves the cell electrical performance. Overall the choice of the operating flow rate in a practical system is a compromise between the pumping energy requirements and equipment cost, the fast and efficient carbon dioxide removal from the cell (i.e. improved gas management), the enhanced and more efficient thermal management of multi-cell stacks, and the electrical performance. Hence, there is no overall optimal operating flow rate and it is more accurate to refer to it as a system specific optimal flow rate.

Attention should be drawn to the model predictions with low flow rates as the results are based on the assumption that the anode side temperature gradient is 0.5°C. As our thermal model [21,22] indicated, and from preliminary results

from our prototype stack, in those cases the temperature gradient could be several degrees, altering slightly the model predictions. In addition the enthalpy for the phase change could be significant in comparison to the total enthalpy of the anode side feed. This limitation will be overcome from our global DMFC engineering model that is currently under development.

Our model has revealed that the anode side inlet temperature drastically affects the vapour–liquid equilibrium and the amount of vapour phase present in the cell (Fig. 8a–c). When the cell is being operated at temperatures below 80–85°C(at $0.5\,dm^3\,min^{-1}$ and $100\,mA\,cm^{-2}$) operation is with a purely liquid fed system as according to the model predictions there is not sufficient carbon dioxide to fully saturate the inlet feed,

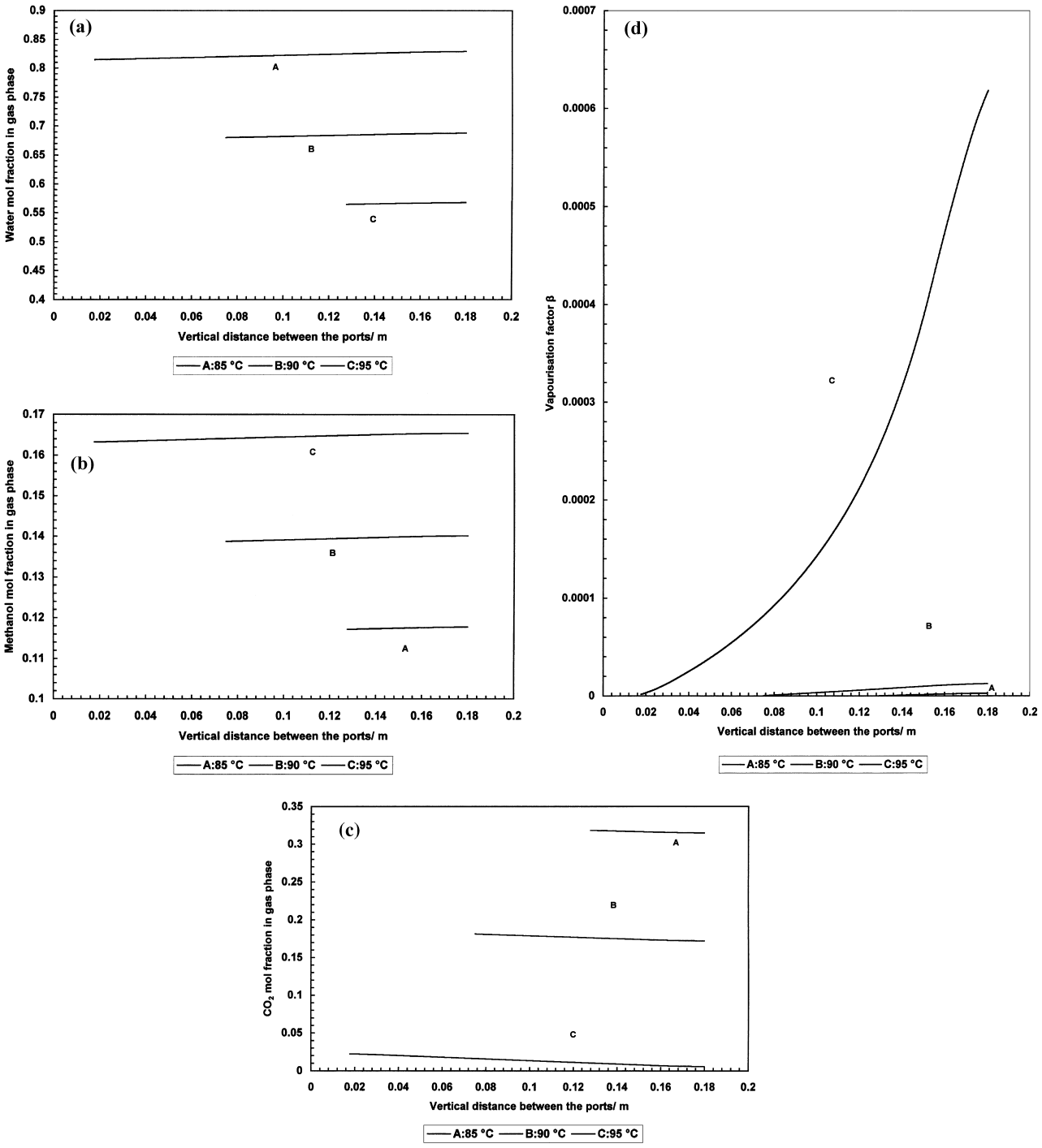

Fig. 8. (a) Water; (b) methanol; (c) carbon dioxide mole fraction β in the gaseous phase and (d) vaporisation factor for a range of operating temperatures (85–95°C) as a function of increasing vertical distance between the ports. (Temperature gradient between inlet and outlet port of 0.5°C, $0.5\,dm^3\,min^{-1}$ $100\,mA\,cm^{-2}$, 2 M solution, active area $270\,cm^2$ unless otherwise stated).

which would eventually lead to the feed boiling. Nevertheless as we have already mentioned in practice the feed will be recycled, hence, there will probably be sufficient carbon dioxide for saturation at some length after the inlet port. As the temperature increases a vapour phase is rapidly formed which is richer in methanol while a significant part of the gaseous phase (above 50%) is water vapour. These results may explain the significant improvement in power performance for the DMFC operated at temperatures near or above 90°C. Fig. 8d shows the significant effect that an increase of temperature has on the vaporisation factor. As expected, as we are going closer to 100°C, the cell is operated more as a vapour fed one with the liquid feed vaporisation immediately after it enters the cell.

3.2. Cathode side fluid compositions

Until recently most of the DMFC development work was carried out for pressurised systems (i.e. for pressurised cathodic compartments) in the range of 0.5–5.0 bar oxygen or air pressure. Some attempts at operating near ambient pressure have been reported but these were limited to small cells due to water management problems. Other groups have reported severe cathode flooding at increased current densities [21,22]. Our group addressed this issue with the aid of the aforementioned individual cell pressure drop behaviour model and found that using a downwards cathode flow configuration, combined with improved flow bed design, eliminates the problem to a great extent.

This kind of practice is also reported by other groups operating cells with low excess stoichiometric (1.2–3 times) air required [3,5]. In addition they have stressed that reducing the air flow rates significantly improves the cells performance by reducing the amount of rejected heat (mainly due to the phase change enthalpy of water and methanol) and greatly reduces the risk of drying out the Nafion® 117 membrane surface which can result in a serious deterioration in its electrical conductivity. We confirmed experimentally such results where the use of an extremely low air flow rate to an unpressurised cell gave electrical performance comparable to a 2 bar air pressure operation (only 2–3% lower with somewhat slower response time).

Fig. 9 shows the model predictions for the gaseous phase mole fractions of every component in the cathode side of the DMFC for a representative case of a cell operating at a current density of 100 mA cm^2, near ambient cathode side pressure, and air flow rate of 1.5 times the stoichiometric required. As can be seen, a significant part of the gaseous phase (almost 75%) is inert nitrogen gas, 15–20% oxygen and the remainder 5–10% is mainly water vapour. Only small amounts of methanol exist in the vapour phase, which is the case for the cathode side in general. The amount of methanol present is not, however, insignificant and must be recovered from the cathode exhaust. The model prediction, however, is sensitive to the model of methanol crossover, data for which is being collected to enable accurate prediction of cathode exhaust gas composition. In practice methanol reacts with the platinum cathode electrocatalyst producing carbon

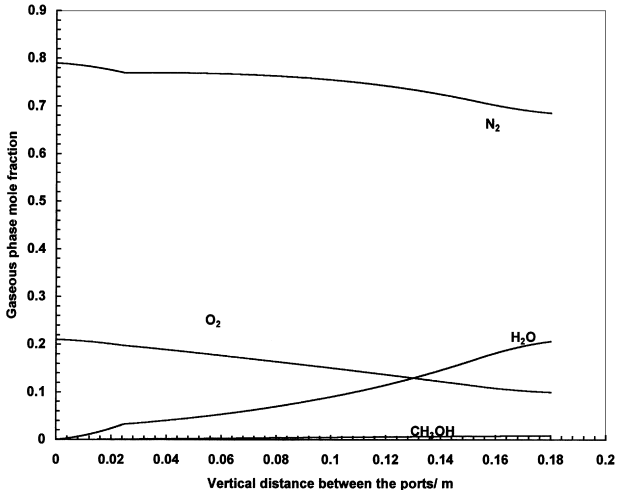

Fig. 9. Cathode side gaseous phase mole fractions (Unpressurised cathode, air inlet temperature 25°C, temperature gradient between the ports 40°C, air excess supply 1.5 the stoichiometry).

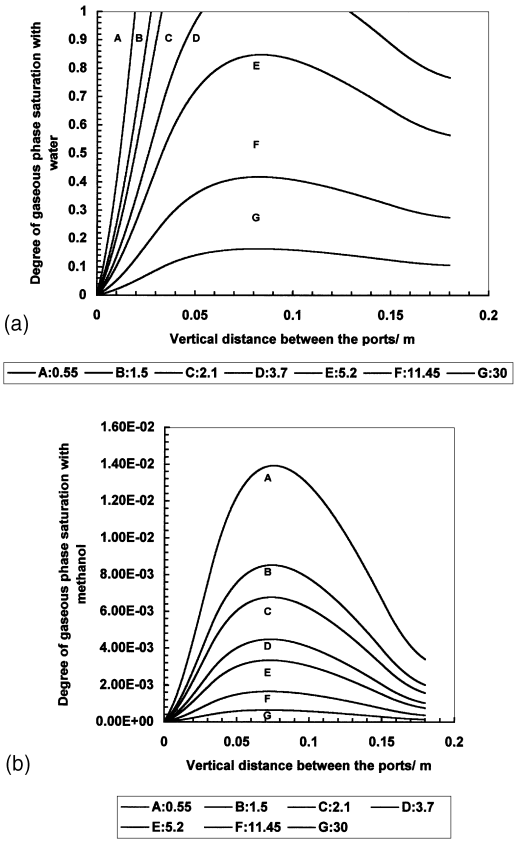

Fig. 10. Degree of cathode side gas saturation for air excess stoichiometry feed as a function of flow bed length (unpressurised cathode, air inlet temperature 25°C, temperature gradient between the ports 40°C). (a) Water saturation; (b) methanol saturation.

dioxide and the parasitic mixed potential that reduces the overall cell electrical performance. The pressure losses for the cathode side are negligible and ranges from 5 Pa for air supply of 0.5 times excess up to 1800 Pa for air excess supply of 30 times the stoichiometric requirements.

Fig. 10a and b show the degree of gas phase saturation with water and methanol, respectively. As is evident low air excess (typically below 1.5 times stoichiometric) is fully saturated, with water, which means that the membrane is well hydrated and hence maintains its good electrical conductivity. As air flow rate increases the cathode air becomes unsaturated with water with all the detrimental effects that this may imply. Overall the model provides a qualitative confirmation of the optimum air excess (between 1.2 and 1.7) reported by Narayanan et al. [3] and with values quoted by Ren et al. (below 3) [5].

4. Conclusions

We have presented a methodology for calculating the chemical equilibrium between the reactants/products flowing in both sides of a DMFC. Based on the local operating conditions we have determined the pressure distribution and the composition of both liquid and gas phases at any point of the flow bed. The conclusions from this study can be summarised as follows:

- Reducing the methanol solution concentration can lead to reduced methanol stripping by carbon dioxide gas (i.e. improved fuel utilisation) and also to reduced methanol crossover.
- The vapour–liquid equilibria of the anode side mainly depend on the anode side inlet temperature and the liquid phase composition, and is very slightly affected by the inlet flow rate.
- Boiling can take place in the flow bed, which can lead, to rapid changes in the vapour–liquid equilibrium and potentially to an electrical performance improvement.
- The cathode side pressure losses are small and hence in a practical DMFC system air can be supplied by an air blower, or potentially, for automobile applications, from the same ‘non energy consuming’ system that supplies air to the ICE.
- Operating the cathode side with extremely low air flow rates (typically below three times but optimal between 1.2 and 1.7 times the stoichiometric required) suggests a significant overall performance improvement is probably due to better membrane hydration.

5. Nomenclature

Symbols

A	VanLaar equation coefficient
B	VanLaar equation coefficient
C	concentration (M)
G	gravitational acceleration ($m\,sec^{-2}$)
G	mass velocity ($kg\,m^{-2}\,s$)
g^E	Gibbs free energy ($kJ\,mol^{-1}$)
H	Henry’s law constant ($M\,10^{-5}$ Pa)
K	hydraulic resistance
K_c	Henry’s law constant
L	liquid phase molar flow ($mol\,s^{-1}$)
N_1	UNIQUAC method coefficient
N_2	UNIQUAC method coefficient
p	partial pressure (Pa)
P	total pressure (Pa)
R	gas constant ($8.31447\,m^3\,Pa\,mol^{-1}\,K$)
T	temperature (K)
x	liquid phase mole fraction
y	gas phase mole fraction
V	vapour phase molar flow ($mol\,s^{-1}$)
Z	total molar flow ($mol\,s^{-1}$)

Greek letters

α	UNIQUAC method coefficient
β	vaporisation factor ($mol\,mol^{-1}$ of inlet feed)
γ	activity coefficient
ε	UNIQUAC method coefficient
ζ	UNIQUAC method coefficient
θ	UNIQUAC method coefficient
χ	Wagner equation coefficient
μ	viscosity ($kg\,m^{-1}\,s$)
ρ	density ($kg\,m^{-3}$)
υ	specific volume ($kg\,m^{-3}$)

Indices

f	liquid
fb	flow bed
fg	liquid–gas
g	gas
gf	gas–liquid
S	saturation point

Acknowledgements

The authors would like to acknowledge the The European Commission for supporting Mr. P. Argyropoulos under a B20 TMR Marie Curie research-training grant and EPSRC for supporting Dr. W.M. Taama.

References

[1] S.R. Narayanan, G. Halpert, W. Chun, B. Jeffries-Nakamura, T.I. Valdez, H. Frank, S. Surampudi. The status of direct methanol fuel cell technology at JPL, in: 37th Power Sources Conference, 1996, Cherry Hill, NJ, USA.

[2] S.R. Narayanan, G. Halpert, W. Chun, B. Jeffries-Nakamura, T.I. Valdez, H. Frank, S. Surampudi, Recent advances in the performance of direct methanol fuel cells, in: Electrochemical Society Annual Meeting, 1996, Los Angeles, CA, USA.

[3] S.R. Narayanan, T. Valdez, N. Rohatgi, W. Chun, G. Halpert, Design of direct methanol fuel cell systems, in: Fuel Cell Seminar, Palm Springs, CA, USA, 1998.
[4] X. Ren, M.S. Wilson, S. Gottesfeld, High performance direct methanol polymer electrolyte fuel cells, J. Electrochem. Soc. 143 (1) (1996) L12–L15.
[5] X. Ren, S.C. Thomas, P. Zelenay, S. Gottesfeld, Direct methanol fuel cells: Developments for portable power and for potential transportation applications, in: Fuel Cell Seminar, 1998, Palm Springs, CA, USA.
[6] K. Scott, W.M. Taama, P. Argyropoulos, Engineering aspects of the direct methanol fuel cell system, J. Power Sources 79 (1) (1999) 43–59.
[7] T.I. Valdez, S.R. Narayanan, H. Frank, W. Chun, Direct methanol fuel cell for portable applications, in: Annual Battery Conference on Applications and Advances, 1997, Long Beach, USA.
[8] J. Cruickshank, K. Scott, The degree and effect of methanol crossover in the direct methanol fuel cell, J. Power Sources 70 (1998) 40–47.
[9] M.K. Ravikumar, Studies on direct methanol fuel cells and nickel–iron batteries, Indian Institute of Science, 1996.
[10] J.T. Wang, J.S. Wainright, R.F. Savinell, M. Litt, A direct methanol fuel cell using acid doped polybenzimidazole as polymer electrolyte, J. Appl. Electrochem. 26 (1996) 751–756.
[11] S. Wasmus, W. Vielstich, Methanol oxidation at carbon supported Pt and Pt–Ru eletctrodes: an on-line MS study using technical electrodes, J. Appl. Electrochem. 23 (1993) 120–124.
[12] K. Scott, W.M. Taama, P. Argyropoulos, Material aspects of the liquid feed direct methanol fuel cell, J. Appl. Electrochem. 28 (12) (1999) 1389–1397.
[13] A.K. Shukla, P.A. Christensen, A. Hamnett, M.P. Hogarth, A vapour-feed direct-methanol fuel cell with proton exchange membrane electrolyte, J. Power Sources 55 (1995) 87–91.
[14] M.P. Hogarth, J. Munk, A.K. Shukla, A. Hamnett, Performance of a carbon-cloth bound porous-carbon electrodes containing an electrodeposited platinum catalyst towards the electrooxidation of the methanol in sulphuric acid electrolyte, J. Appl. Electrochem. 24 (1994) 85–88.
[15] M.P. Hogarth, G.A. Hards, Direct methanol fuel cells: technological advances and further requirements, Platinum Metals Rev. 40 (4) (1996) 150–159.
[16] M. Hogarth, P.A. Christensen, A. Hamnett, A. Shukla, The design and construction of high performance direct methanol fuel cells. 1. Liquid feed systems, J. Power Sources 69 (1997) 113–124.
[17] M. Hogarth, P. Christensen, A. Hamnett, A.K. Shukla, The design and construction of high performance direct methanol fuel cells. 2. Vapour feed systems, J. Power Sources 69 (1997) 125–136.
[18] P. Argyropoulos, K. Scott, W.M. Taama, Pressure drop modelling for liquid feed direct methanol fuel cells (DMFCs). Part I. Model development, Chem. Eng. J. 73 (3) (1999) 217–227.
[19] P. Argyropoulos, K. Scott, W.M. Taama, Engineering and modeling aspects on large scale liquid feed DMFC stacks, in: Proceedings of the 5th European Symposium on Electrochemical Engineering, IChemE, 1999, Exeter, UK.
[20] P. Argyropoulos, K. Scott, W.M. Taama, Pressure drop modelling for liquid feed direct methanol fuel cells (DMFCs). Part II. Model based parametric analysis, Chem. Eng. J. 73 (3) (1999) 229–245.
[21] P. Argyropoulos, K. Scott, W.M. Taama, One dimensional thermal model for DMFC stacks. Part I. Model development, J. Power Sources 79 (2) (1999) 169–183.
[22] P. Argyropoulos, K. Scott, W.M. Taama, One dimensional thermal model for DMFC stacks. Part II. Model based parametric analysis and predicted temperature profiles, J. Power Sources 79 (2) (1999) 184–198.
[23] P. Argyropoulos, K. Scott, W.M. Taama, Modeling reactants and products flow distribution for internally man folded DMFC stacks, J. Fluids Eng., 1999.
[24] P. Argyropoulos, K. Scott, W.M. Taama, Hydrodynamic modeling of direct methanol fuel cell stacks, J. Appl. Electrochem., 1999.
[25] K. Sundmacher, K. Scott, The impact of electrosmotic and pressure-driven mass transport on the limiting currents of a liquid-fed direct methanol polymer electrolyte fuel cell, Chem. Eng. Sci., 1998, in press.
[26] K. Sundmacher, K. Scott, Electrochemical oxidation of methanol in a polymer electrolyte fuel cell: modelling and experimental validation of current-voltage characteristics, in: Proceedings of the IChemE Research Event, 1998, Newcastle upon Tyne, UK.
[27] R.C. Reid, J.M. Prausnitz, B.E. Poling, The Properties of Gases and Liquids, 4th Edition, McGraw-Hill, New York, 1987.
[28] R.H. Perry, D.W. Green, J.O. Maloney, Perry's Chemical Engineers' Handbook, 6th International Edition, McGraw Hill, Singapore, 1984.
[29] Y.S. Won, D.K. Chung, A.F. Mills, Density, viscocity, surface tension and carbon dioxide solubility and diffusivity of methanol, ethanol, aqueous propanol, and aqueous ethylene glycol at 25°C, J. Chem. Eng. Data 26 (2) (1981) 140–141.
[30] S. Sandler, Chemical and Engineering Thermodynamics, 2nd Edition, Wiley, New York, 1989.
[31] S.M. Walas, in: H. Brenner (Ed.), Chemical Process Equipment: Selection and Design. Butterworth-Heinemann Series in Chemical Engineering, Butterworth-Heinemann, Boston, USA, 1990.
[32] P. Argyropoulos, K. Scott, W.M. Taama, Gas evolution and power performance in direct methanol fuel cells, J. Appl. Electrochem. 29 (1999) 661–669.
[33] K. Scott, R. Reeves, P.A. Christensen, in preparation.